Study of the resonance contributions in the $\Xi_b^- \to pK^-K^-$ decay

Zhong-Yu Wang,[1,2,*] Si-Qiang Luo,[1,2,†] Zhi-Feng Sun,[1,2,3,4,‡] C. W. Xiao,[5,§] and Xiang Liu[1,2,3,4,‖]

[1]School of Physical Science and Technology, Lanzhou University, Lanzhou 730000, China
[2]Lanzhou Center for Theoretical Physics, Lanzhou University, Lanzhou 730000, China
[3]Research Center for Hadron and CSR Physics, Lanzhou University and Institute of Modern Physics of CAS, Lanzhou 730000, China
[4]Key Laboratory of Theoretical Physics of Gansu Province, and Frontiers Science Center for Rare Isotopes, Lanzhou University, Lanzhou 730000, China
[5]School of Physics and Electronics, Hunan Key Laboratory of Nanophotonics and Devices, Central South University, Changsha 410083, China

(Received 1 July 2022; accepted 16 November 2022; published 29 November 2022)

The decay process $\Xi_b^- \to pK^-K^-$ is studied with the final-state interaction approach by considering the contributions from the S-wave meson-baryon interactions, and also the intermediate state $\Lambda(1520)$ in the D-wave. The low-lying resonances $\Lambda(1405)$ and $\Lambda(1670)$ have significant contributions, which are both dynamically generated from the S-wave final-state interactions with isospin $I = 0$. Furthermore, the $\Lambda(1520)$ state also has important contributions from D-wave. With these resonances contributions, the experimental data of the lower pK^- invariant mass distributions are well-described. We also discuss the contribution of another resonance in the S-wave with isospoin $I = 1$, which cannot be ignored. Moreover, some of the branching fractions obtained for the corresponding decay channels are consistent with the experimental measurements.

DOI: 10.1103/PhysRevD.106.096026

I. INTRODUCTION

The weak decays of charmed and bottomed hadrons can not only be used to explore the CP-violation phenomena and new physics beyond the standard model, but also be suitable for exploring the nature of the intermediate resonances. In particular, the three-body decays of charmed and bottomed hadrons provide a good chance to study the properties of the intermediate resonances, and also a good opportunity to observe new resonances in the invariant mass spectra of the final states. It is well-known that in 2015 the LHCb Collaboration reported two pentaquarklike resonances, i.e., $P_c(4380)^+$ and $P_c(4450)^+$ in the $J/\psi p$ invariant mass spectrum of the $\Lambda_b^0 \to J/\psi K^- p$ decay [1,2], which was confirmed by a model-independent analysis of the data [3] and in the $\Lambda_b^0 \to J/\psi p\pi^-$ decay [4]. Furthermore, using the data of Run I and Run II, in 2019 the LHCb Collaboration updated their results for the $\Lambda_b^0 \to J/\psi K^- p$ decay, where in fact three clear narrow structures, i.e., $P_c(4312)^+$, $P_c(4440)^+$ and $P_c(4457)^+$, were found [5]. Therefore, in recent years a large number of three-body charmed and bottomed baryons' decays, e.g., Λ_c and Λ_b decays, have caught much attention experimentally [6–12], where more discussions about the theoretical and experimental progress on this issue can be found in the recent reviews [13–18], and references therein. In Ref. [19], two Ξ states, $\Xi(1620)^0$ and $\Xi(1690)^0$, were found in the $\Xi_c^+ \to \Xi^-\pi^+\pi^+$ decay. In the $\Lambda_b^0\pi^+\pi^-$ mass spectrum, two narrow resonances $\Lambda_b(6146)^0$ and $\Lambda_b(6152)^0$ were reported in Ref. [20] and another wide one was found in Ref. [21]. Moreover, the three-body decays of the Ξ_b state have also caught much attentions. In 2017, the $\Xi_b^- \to J/\psi\Lambda K^-$ decay was first observed by the LHCb Collaboration [22] with the suggestion of Ref. [23] to look for the hidden-charm pentaquark states with open strangeness as predicted in Refs. [24–27]. Indeed in 2021, the $P_{cs}(4459)^0$ state was observed in the $J/\psi\Lambda$ invariant mass distributions of the $\Xi_b^- \to J/\psi\Lambda K^-$ decay [28]. In the same year, the $\Omega_b^- \to \Xi_c^+ K^-\pi^-$ decay was investigated by the LHCb Collaboration [29], where four structures were observed in the $\Xi_c^+ K^-$ invariant mass distributions, i.e., $\Omega_c(3000)^0$, $\Omega_c(3050)^0$, $\Omega_c(3065)^0$, and $\Omega_c(3090)^0$, which were consistent with the previous measurements of the LHCb Collaboration [30] and the Belle Collaboration [31]. Besides, the LHCb Collaboration had performed the

*zhongyuwang@foxmail.com
†luosq15@lzu.edu.cn
‡sunzf@lzu.edu.cn
§xiaochw@csu.edu.cn
‖xiangliu@lzu.edu.cn

amplitude analysis in Ref. [32] for the decay $\Xi_b^- \to pK^-K^-$, which was reported for the first time in 2017 [33], and where the CP-violation effect was discussed and the contributions from the resonances $\Sigma(1385)$, $\Lambda(1405)$, $\Lambda(1520)$, etc., were found. In the present work, this three-body decay, i.e., $\Xi_b^- \to pK^-K^-$, catches our interests to study the nature of the intermediate resonances in this decay process.

Indeed, the motivation of studying the $\Xi_b^- \to pK^-K^-$ decay [33] was to look for CP-violation in the b-baryon decays, which was also concerned in theories [34,35]. Even though the CP-violation effect was not found with the amplitude analysis in Ref. [32], as a byproduct they reported that the resonances $\Sigma(1385)$, $\Lambda(1405)$, $\Lambda(1520)$, etc., had significant contributions to the decay amplitude. $\Lambda(1520)$ and $\Lambda(1670)$ were observed with significance more than 5σ, which motivated us to investigate (theoretically) the contributions of the states $\Lambda(1405)$ and $\Lambda(1670)$ in the present work. Although the $\Lambda(1405)$ resonance was predicted and observed more than 60 years ago [36–38], its structure and properties are still under debate. It was considered to be the normal three-quark baryon in the quark model [39–41], but the mass obtained was higher than the experimental result [42]. On the other hand, it was confusing that the mass of the $\Lambda(1405)$ was significantly lighter than the lowest nonstrange negative-parity baryons $N(1520)$ [43]. Meanwhile, the $\Lambda(1405)$ was dynamically produced in the coupled-channel interactions [44–46] based on the interaction potentials from the chiral dynamics, where the experimental data for the cross sections were well-described. Note that, Ref. [46] only used one free parameter in the loop functions, where the on shell approximations were taken [47], and obtained consistent results for the cross sections and the other experimental data. Later, with the same method, which is also called the chiral-unitary approach (ChUA) [48–51], the $\Lambda(1670)$ state was also dynamically generated in the strangeness $S = -1$ and the isospin $I = 0$ sector [52] and assumed to be a bound state of the $K\Xi$ channel. Remarkably the two-pole structure for the $\Lambda(1405)$ state was found for the first time in the coupled-channel interactions with the quark bag model [53]. Furthermore, the two-pole structure of the $\Lambda(1405)$ was investigated in detail using the ChUA in Refs. [49,54–62]. However, the cross sections of the transition $K^-p \to \eta\Lambda$ were measured by the Crystal Ball Collaboration [63], which supported the picture of three-quark baryon for the $\Lambda(1670)$ state. In the chiral-quark model, the $\Lambda(1670)$ in Ref. [64] could also be treated as a three-quark state based on the analysis of the data of the $K^-p \to \pi^0\Sigma^0$ reaction [65]. Thus, the structures and properties of the $\Lambda(1405)$ and $\Lambda(1670)$ are still with a lot of controversies.

Recently, in Ref. [61] with the ChUA we systematically revisited the interactions of the $\bar{K}N$ and its coupled channels, and the single-channel interactions of the channels $\bar{K}N$ and $\pi\Sigma$, respectively, where the nature of the $\Lambda(1405)$ was discussed and that it was really two poles of the second Riemann sheet or two molecular states. The latest experimental results of the $\Xi_b^- \to pK^-K^-$ decay in Ref. [32] can probe the properties of the resonances $\Lambda(1405)$, $\Lambda(1520)$, and $\Lambda(1670)$. Based on the two-body interaction results of Ref. [61], we can investigate the $\Xi_b^- \to pK^-K^-$ decay with the final-state interaction (FSI) approach and try to hint at the molecular nature of the states $\Lambda(1405)$ and $\Lambda(1670)$. More discussions about these molecular states can be found in the review of Ref. [16]. Note that, since the $\Lambda(1520)$ state is located between the above two resonances and has a significant contribution in the energy region that we are interested in. We also take into account in our formalism and ignore the less contribution resonances, such as the ones $\Sigma(1385)$, $\Sigma(1775)$, $\Sigma(1915)$, and so on, as found in Ref. [32]. Using a realistic chiral meson-baryon amplitude for the final-state interactions, Ref. [66] predicted the line shapes of the $\pi\Sigma$ spectrum of the $\Xi_b^0 \to D^0\pi\Sigma$ decay, which showed that the structure of the $\Lambda(1405)$ was destroyed by the interference between the direct generation and rescattering procedures. One can look forward to what we get from the $\Xi_b^- \to pK^-K^-$ decay with the FSI under the ChUA, which is a useful approach, such as a hidden charmed pentaquark state with strangeness predicted in the decay of $\Xi_b^- \to J/\psi\Lambda K^-$ in Ref. [23] as mentioned above, which was confirmed by experiment [28]. More discussions and applications for the heavy baryons three-body decays with the FSI based on the ChUA can be found in Refs. [67–71].

Our work is organized as follows. In Sec. II, we will introduce the formulas of the decay amplitudes with the FSI and the ChUA. Next, our results are shown in Sec. III. At the end, a short conclusion is made in Sec. IV.

II. FORMALISM

In the present work, we investigate the weak-decay process of $\Xi_b^- \to pK^-K^-$, taking into account the FSI of K^-p with its coupled channels. The most important contribution of the weak-decay process comes from the W-external emission mechanism based on topological classification [72,73]. Thus, we only consider the dominant mechanism as shown in Fig. 1, and omit the other contributions such as W-internal emission, W-exchange, W-annihilation, etc.,[1] which are suppressed by the color factor [67,75]. As shown in Fig. 1, the ds quark pair in the Ξ_b^- has spin $S = 0$ and has the flavor wave function $\frac{1}{\sqrt{2}}(ds - sd)$, which is the most attractive "good" diquark and can be assumed as a spectator in the weak-decay process [67,76]. Meanwhile, the b quark in the Ξ_b^- decays into the u quark via an external emission W^- boson. Then the W^- boson creates the $\bar{u}$ and s quarks, which eventually form a K^- meson. The remaining quarks $\frac{1}{\sqrt{2}}u(ds - sd)$ are

[1]In fact, these mechanisms can be obtained by rearranging the quark lines of Fig. 1 or considering the absorption diagrams [72], see more discussions in Refs. [67,74].

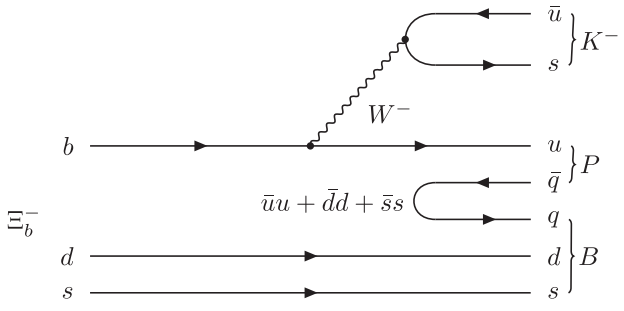

FIG. 1. The dominant diagram for the $\Xi_b^- \to pK^-K^-$ decay with the W-external emission mechanism, where P and B represent the pseudoscalar mesons and baryons, respectively.

hadronized by introducing the quark pairs $(\bar{u}u + \bar{d}d + \bar{s}s)$ from the vacuum to form a meson and a baryon, as depicted in Fig. 1. We know that the Ξ_b^- state has the quark components with a flavor function as

$$|\Xi_b^-\rangle \equiv \frac{1}{\sqrt{2}}|b(ds - sd)\rangle, \tag{1}$$

and after the b quark decays into the u quark, we have the uds cluster, proceeded as

$$|H\rangle = V_P V_{ub} V_{us} \frac{1}{\sqrt{2}}|u(ds - sd)\rangle, \tag{2}$$

where V_P represents the vertex factor of the weak decay for the $\bar{q}q$ pair creation, which is assumed to be a constant, independent on the invariant mass in our calculation. More details can be seen in Refs. [77,78]. The $V_{q_1q_2}$ represents the element of the Cabibbo-Kobayashi-Maskawa (CKM) matrix for the transition of $q_1 \to q_2$ quarks. With the formation of K^- meson by the $\bar{u}$ and s quarks from the W^- boson, the spectators, the d and s quarks, become a part of the light baryon and the u quark from b decay becomes a part of the meson combining the $\bar{q}q$ pair generated from the vacuum. These processes are formulated as

$$\begin{aligned}|H\rangle &= V_P V_{ub} V_{us} \frac{1}{\sqrt{2}}|u(\bar{u}u + \bar{d}d + \bar{s}s)(ds - sd)\rangle \\ &= V_P V_{ub} V_{us} \frac{1}{\sqrt{2}} \sum_{i=1}^{3} |P_{1i} q_i (ds - sd)\rangle,\end{aligned} \tag{3}$$

where the q_i is the quark field and the P_{ij} is the $q\bar{q}$ pair matrix element as follows:

$$q \equiv \begin{pmatrix} u \\ d \\ s \end{pmatrix}, \qquad P = \begin{pmatrix} u\bar{u} & u\bar{d} & u\bar{s} \\ d\bar{u} & d\bar{d} & d\bar{s} \\ s\bar{u} & s\bar{d} & s\bar{s} \end{pmatrix}. \tag{4}$$

The $SU(3)$ matrices for the pseudoscalar mesons and the lowest-lying baryon octet can also be represented by the corresponding hadron fields, i.e.,

$$P = \begin{pmatrix} \frac{1}{\sqrt{2}}\pi^0 + \frac{1}{\sqrt{3}}\eta + \frac{1}{\sqrt{6}}\eta' & \pi^+ & K^+ \\ \pi^- & -\frac{1}{\sqrt{2}}\pi^0 + \frac{1}{\sqrt{3}}\eta + \frac{1}{\sqrt{6}}\eta' & K^0 \\ K^- & \bar{K}^0 & -\frac{1}{\sqrt{3}}\eta + \sqrt{\frac{2}{3}}\eta' \end{pmatrix}, \tag{5}$$

$$B = \begin{pmatrix} \frac{1}{\sqrt{2}}\Sigma^0 + \frac{1}{\sqrt{6}}\Lambda & \Sigma^+ & p \\ \Sigma^- & -\frac{1}{\sqrt{2}}\Sigma^0 + \frac{1}{\sqrt{6}}\Lambda & n \\ \Xi^- & \Xi^0 & -\frac{2}{\sqrt{6}}\Lambda \end{pmatrix}. \tag{6}$$

In Eq. (5), we take the standard mixing of the η and η' in terms of a singlet and an octet of $SU(3)$. Then the hadronization processes in the quark level can be accomplished to the hadron level in terms of a pseudoscalar meson and a baryon, we obtain the final meson-baryon states for the hadronization procedure, given by

$$\begin{aligned}|H\rangle = V_P V_{ub} V_{us} \Big(&\frac{1}{2}|\pi^0\Sigma^0\rangle + \frac{1}{2\sqrt{3}}|\pi^0\Lambda\rangle + \frac{1}{\sqrt{6}}|\eta\Sigma^0\rangle \\ &+ \frac{1}{3\sqrt{2}}|\eta\Lambda\rangle + |\pi^+\Sigma^-\rangle + |K^+\Xi^-\rangle\Big),\end{aligned} \tag{7}$$

where we neglect the irrelevant η' state since it is too massive and has no effect on the low-energy region in the present work. The flavor functions of the mesons and baryons we used are the same as the ones in the Appendix of Ref. [74]. It is obvious that there is no K^-p state directly produced in the tree level of the Ξ_b^- decay based on the mechanism of Fig. 1. However, the final meson-baryon states can go to further FSI, as depicted in Fig. 2. The corresponding amplitudes with the contributions from the rescattering mechanism can be written as

$$\mathcal{M}_{S-\text{wave}}(M_{12},M_{13}) = \mathcal{D}\Big[\frac{1}{2}G_{\pi^0\Sigma^0}(M_{12})T_{\pi^0\Sigma^0\to K^-p}(M_{12}) + \frac{1}{2\sqrt{3}}G_{\pi^0\Lambda}(M_{12})T_{\pi^0\Lambda\to K^-p}(M_{12}) + \frac{1}{\sqrt{6}}G_{\eta\Sigma^0}(M_{12})T_{\eta\Sigma^0\to K^-p}(M_{12}) + \frac{1}{3\sqrt{2}}G_{\eta\Lambda}(M_{12})T_{\eta\Lambda\to K^-p}(M_{12}) + G_{\pi^+\Sigma^-}(M_{12})T_{\pi^+\Sigma^-\to K^-p}(M_{12}) + G_{K^+\Xi^-}(M_{12})T_{K^+\Xi^-\to K^-p}(M_{12}) + (2\leftrightarrow 3)\Big], \tag{8}$$

where $\mathcal{D}$ is a free parameter, which can be determined later by fitting the experimental data and have absorbed the vertex factor V_P, the elements of CKM matrix V_{ub}, V_{us}, and a global constant C to match the events of the experimental data. Note that, we use the label 1 for the proton, label 2 for the K^- from the same vertex as the proton, and label 3 for the other K^- directly created by the W-boson. The symbol $(2\leftrightarrow 3)$ means exchanging the labels 2 and 3 in the amplitude $\mathcal{M}_{S-\text{wave}}$, which represents the symmetry of identical particles K^-K^- in the final states. M_{ij} is the energy of two particles in the center-of-mass frame. G_{PB} and $T_{PB\to P'B'}$ are the loop functions and the scattering amplitudes, respectively, which will be introduced later and where P and B stand for the pseudoscalar meson and baryon, respectively.

Note that the final states K^-p are contributed with isospins both $I=0$ and $I=1$. We calculate the rescattering amplitudes in the isospin basis. For the isospin $I=0$, the four coupled channels $\bar{K}N$, $\pi\Sigma$, $\eta\Lambda$ and $K\Xi$ need to be considered. For the isospin $I=1$, there are five coupled channels $\bar{K}N$, $\pi\Sigma$, $\pi\Lambda$, $\eta\Sigma$, and $K\Xi$. Then we decompose the amplitudes of the physical states in Eq. (8) into the ones with the isospin states, shown as

$$\begin{aligned}
T_{\pi^0\Sigma^0\to K^-p} &= -\frac{1}{\sqrt{6}}T^{I=0}_{\pi\Sigma\to\bar{K}N}, \quad T_{\pi^0\Lambda\to K^-p} = -\frac{1}{\sqrt{2}}T^{I=1}_{\pi\Lambda\to\bar{K}N},\\
T_{\eta\Sigma^0\to K^-p} &= -\frac{1}{\sqrt{2}}T^{I=1}_{\eta\Sigma\to\bar{K}N}, \quad T_{\eta\Lambda\to K^-p} = \frac{1}{\sqrt{2}}T^{I=0}_{\eta\Lambda\to\bar{K}N},\\
T_{\pi^+\Sigma^-\to K^-p} &= \frac{1}{2}T^{I=1}_{\pi\Sigma\to\bar{K}N} - \frac{1}{\sqrt{6}}T^{I=0}_{\pi\Sigma\to\bar{K}N},\\
T_{K^+\Xi^-\to K^-p} &= \frac{1}{2}T^{I=1}_{K\Xi\to\bar{K}N} - \frac{1}{2}T^{I=0}_{K\Xi\to\bar{K}N},
\end{aligned} \tag{9}$$

where we have used the phase convention for the mesons $|\pi^+\rangle = -|1,1\rangle$, $|K^-\rangle = -|1/2,-1/2\rangle$, and for the baryons $|\Sigma^+\rangle = -|1,1\rangle$, $|\Xi^-\rangle = -|1/2,-1/2\rangle$ in terms of isospin states as used in Ref. [46].

In addition, the rescattering amplitude $T_{PB\to P'B'}$ can be obtained by solving the coupled channel Bethe-Salpeter equations of the on shell form

$$T = [1 - VG]^{-1}V, \tag{10}$$

where G is a diagonal matrix composed of meson-baryon loop functions. The element of the G matrix with the dimensional regularization is given by [55]

$$\begin{aligned}
G_{PB}(M_{\text{inv}}) = \frac{2m_B}{16\pi^2}\Big\{ & a_{PB}(\mu) + \ln\frac{m_B^2}{\mu^2} + \frac{m_P^2 - m_B^2 + M_{\text{inv}}^2}{2M_{\text{inv}}^2}\ln\frac{m_P^2}{m_B^2} + \frac{q_{cm}(M_{\text{inv}})}{M_{\text{inv}}}\big[\ln\left(M_{\text{inv}}^2 - (m_B^2 - m_P^2) + 2q_{cm}(M_{\text{inv}})M_{\text{inv}}\right)\\
& + \ln\left(M_{\text{inv}}^2 + (m_B^2 - m_P^2) + 2q_{cm}(M_{\text{inv}})M_{\text{inv}}\right) - \ln\left(-M_{\text{inv}}^2 - (m_B^2 - m_P^2) + 2q_{cm}(M_{\text{inv}})M_{\text{inv}}\right)\\
& - \ln\left(-M_{\text{inv}}^2 + (m_B^2 - m_P^2) + 2q_{cm}(M_{\text{inv}})M_{\text{inv}}\right)\big]\Big\},
\end{aligned} \tag{11}$$

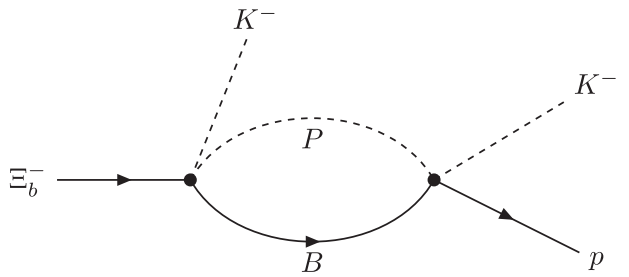

FIG. 2. The diagram for the pseudoscalar meson (P) and baryon (B) final state interactions via the rescattering mechanism.

where M_{inv} is the invariant mass of the meson-baryon system in the coupled channels, and m_P (m_B) is the mass of the intermediate pseudoscalar meson (baryon). The μ is the scale of dimensional regularization, following Refs. [52,55,61], which is taken as 0.63 GeV, and $a_{PB}(\mu)$ is the subtraction constant, taken as

$$\begin{aligned}
a_{\bar{K}N} &= -1.84, \quad a_{\pi\Sigma} = -2.00, \quad a_{\pi\Lambda} = -1.83,\\
a_{\eta\Lambda} &= -2.25, \quad a_{\eta\Sigma} = -2.38, \quad a_{K\Xi} = -2.67.
\end{aligned} \tag{12}$$

In order to study the properties of the intermediate resonances produced in the two-body interactions of the final

states, these parameters are not regarded as free ones in our calculation, see Ref. [78] for more discussions. Besides, $q_{cm}(M_{\rm inv})$ is the three-momentum of the particle in the center-of-mass frame,

$$q_{cm}(M_{\rm inv}) = \frac{\lambda^{1/2}(M_{\rm inv}^2, m_P^2, m_B^2)}{2M_{\rm inv}}, \tag{13}$$

with the usual Källen triangle function $\lambda(a,b,c) = a^2+b^2+c^2-2(ab+ac+bc)$.

Furthermore, the matrix V denotes the S-wave interaction potentials for the coupled channels of $\bar{K}N$, of which the elements are taken from the lowest order chiral Lagrangian [79–81]. Finally, the expressions for them are given by [52]

$$V_{ij}(M_{\rm inv}) = -C_{ij}\frac{1}{4f^2}(2M_{\rm inv}-m_i-m_j) \times \left(\frac{m_i+E_i}{2m_i}\right)^{1/2}\left(\frac{m_j+E_j}{2m_j}\right)^{1/2}, \tag{14}$$

where the m_i, m_j are the masses of the initial and final baryons, and E_i, E_j the energies of the initial and final mesons. For the meson decay constant, we take $f = 1.123 f_\pi$, where the $f_\pi = 0.093$ GeV is the pion decay constant. The coefficient matrix elements C_{ij} are symmetric, $C_{ij} = C_{ji}$, given in Table I for the $I = 0$ sector, and in Table II for the $I = 1$ sector, which are taken from Ref. [46].

In addition, the *uds* cluster in Fig. 1 can form intermediate particles directly and then decay into the final states $K^- p$. As implied in the experimental results of the LHCb Collaboration [32], we consider the contributions of the intermediate state $\Lambda(1520)$ as shown in Fig. 3. The effective Lagrangians for the decay $\Xi_b^- \to \Lambda(1520)K^- \to pK^-K^-$ in Fig. 3 are defined in general following [82], where the weak interaction vertex is given by

$$\mathcal{L}^{\rm weak}_{K\Xi_b\Lambda^*} = \frac{i}{m_K}(\bar{\Lambda}^*_\mu)(\partial^\mu K)(g^{\rm PV}_{K\Xi_b\Lambda^*} - g^{\rm PC}_{K\Xi_b\Lambda^*}\gamma_5)\Xi_b + {\rm H.c.}, \tag{15}$$

where $g^{\rm PV}_{K\Xi_b\Lambda^*}$ and $g^{\rm PC}_{K\Xi_b\Lambda^*}$ are the parity-violating (PV) and parity-conserving (PC) couplings, respectively. To reduce theoretical uncertainties, we assume $g^{\rm PV}_{K\Xi_b\Lambda^*} = g^{\rm PC}_{K\Xi_b\Lambda^*} = g_{K\Xi_b\Lambda^*}$. The strong-interaction vertex is written as

$$\mathcal{L}^{\rm strong}_{K\Lambda^* p} = -\frac{ig_{K\Lambda^* p}}{m_K}(\bar{\Lambda}^*_\mu\gamma_5)(\partial^\mu K)p + {\rm H.c.}. \tag{16}$$

Using the above effective Lagrangians and the Breit-Wigner propagator [35,83], we can get the amplitude corresponding to Fig. 3 as follows:

$$\mathcal{M}_{\Lambda^*}(M_{12}) = -\frac{g_{K\Lambda^* p}}{m_K^2}\frac{\bar{u}_p\gamma_5[\Delta_{\mu\nu}(M_{12})k_2^\mu k_3^\nu](g_{K\Xi_b\Lambda^*} - g_{K\Xi_b\Lambda^*}\gamma_5)u_{\Xi_b^-}}{M_{12}^2 - m_{\Lambda^*}^2 + i\Gamma_{\Lambda^*}m_{\Lambda^*}}, \tag{17}$$

where $\Delta_{\mu\nu}(q)$ is the projection operator of spin $S = 3/2$, given by

TABLE I. The coefficient matrix elements C_{ij} in Eq. (14) for $I = 0$ sector.

C_{ij}	$\bar{K}N$	$\pi\Sigma$	$\eta\Lambda$	$K\Xi$
$\bar{K}N$	3	$-\sqrt{\frac{3}{2}}$	$\frac{3}{\sqrt{2}}$	0
$\pi\Sigma$		4	0	$\sqrt{\frac{3}{2}}$
$\eta\Lambda$			0	$-\frac{3}{\sqrt{2}}$
$K\Xi$				3

TABLE II. The coefficient matrix elements C_{ij} in Eq. (14) for $I = 1$ sector.

C_{ij}	$\bar{K}N$	$\pi\Sigma$	$\pi\Lambda$	$\eta\Sigma$	$K\Xi$
$\bar{K}N$	1	−1	$-\sqrt{\frac{3}{2}}$	$-\sqrt{\frac{3}{2}}$	0
$\pi\Sigma$		2	0	0	1
$\pi\Lambda$			0	0	$-\sqrt{\frac{3}{2}}$
$\eta\Sigma$				0	$-\sqrt{\frac{3}{2}}$
$K\Xi$					1

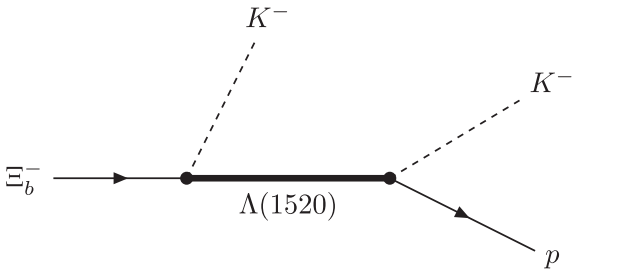

FIG. 3. The $\Xi_b^- \to pK^-K^-$ decay via the intermediate state $\Lambda(1520)$.

$$\Delta_{\mu\nu}(q) = (\not{q} + m_{\Lambda^*})\left[g_{\mu\nu} - \frac{1}{3}\gamma_\mu\gamma_\nu - \frac{1}{3m_{\Lambda^*}}(\gamma_\mu q_\nu - \gamma_\nu q_\mu) - \frac{2}{3m^2_{\Lambda^*}} q_\mu q_\nu\right]. \tag{18}$$

However, note that the $\Lambda(1520)$ state has the structure and can not be regarded as a pointlike particle. Thus, we introduce the following form factor developed in Refs. [84,85] into the $\Lambda(1520)$ amplitude,

$$F(M_{ij}) = \frac{\Lambda^4}{\Lambda^4 + (M^2_{ij} - m^2_{\Lambda(1520)})^2}, \tag{19}$$

where Λ stands for a phenomenological cutoff parameter, which is taken as 1 GeV [86]. In fact, this parameter has almost no effect on our fit, and it mainly influences the high-energy region. Taking into account the symmetry of identical particles K^-K^- in the final states, we get the final amplitude for the $\Lambda(1520)$ contributions,

$$\mathcal{M}_{\Lambda(1520)}(M_{12}, M_{13}) = -\frac{\mathcal{D}_{\Lambda(1520)}}{m^2_K} \frac{\bar{u}_p\gamma_5[\Delta_{\mu\nu}(M_{12})k_2^\mu k_3^\nu](1-\gamma_5)u_{\Xi_b^-}}{M^2_{12} - m^2_{\Lambda(1520)} + i\Gamma_{\Lambda(1520)}m_{\Lambda(1520)}} F(M_{12}) + (2 \leftrightarrow 3), \tag{20}$$

where $\mathcal{D}_{\Lambda(1520)}$ is a free parameter, which also can be determined by fitting the experimental data the collected couplings $g_{K\Xi_b\Lambda^*}$, $g_{K\Lambda^* p}$, and a global constant C to match the events of the experimental data. Besides, the mass of $\Lambda(1520)$ is taken as $m_{\Lambda(1520)} = 1.519$ GeV, and the width of the $\Lambda(1520)$ is taken as $\Gamma_{\Lambda(1520)} = 0.016$ GeV, which are taken from the Particle Data Group (PDG) [87]. Note that, the variables M_{ij} are not completely independent, they fulfill the following constraint condition, which means that only two of them are independent,

$$M^2_{12} + M^2_{13} + M^2_{23} = m^2_{\Xi_b^-} + m^2_p + m^2_{K^-} + m^2_{K^-}. \tag{21}$$

Finally, the three-body double differential width distribution for the $\Xi_b^- \to pK^-K^-$ decay is given by [87]

$$\frac{d^2\Gamma}{dM_{12}dM_{13}} = \frac{1}{(2\pi)^3}\frac{M_{12}M_{13}}{8m^3_{\Xi_b^-}}\frac{1}{2}(|\mathcal{M}_{S-\text{wave}}|^2 + |\mathcal{M}_{\Lambda(1520)}|^2), \tag{22}$$

where there is a factor of $1/2$, since the two K^- are identical. Since the $\Lambda(1520)$ contributes in the D-wave, we take an incoherent sum for the contributions of the S-wave and the $\Lambda(1520)$ due to no interference between different partial waves under the orthogonality relation, where one should keep in mind that the scattering amplitudes of the coupled channels evaluated by Eq. (10) are pure S-wave. This is different from the experimental modeling, where the nonzero unphysical interference would occur due to the symmetrization of the Dalitz plot as discussed in Ref. [32]. Thus, these interference effects would lead to the source of systematic uncertainties, but there is no such interference effect in our formalism. Furthermore, since the states $\Lambda(1405)$, $\Lambda(1670)$, and a new state with isospin $I = 1$ (see the results later) are dynamically generated in the same sector of the coupled-channel interactions; the interference effect has been contained in the scattering amplitudes, see Eq. (8), where more discussions can be found in Ref. [88]. In the present work, we aim at understanding the molecular nature of these S-wave low-lying resonances. Thus, we calculate the invariant mass spectrum $d\Gamma/dM_{12}$ by integrating the variable M_{13} in Eq. (22). In Sec. III, we also evaluate the distribution $d\Gamma/dM_{23}$ through Eq. (21).

III. RESULTS

As mentioned in the introduction, the LHCb Collaboration had measured the decay process $\Xi_b^- \to pK^-K^-$, where the pK^- invariant mass spectrum was given. Note that the two identical K^- mesons lead to M_{12} and M_{13} having a symmetry under interchanging the variables, thus the experimental results are described by $M^{\text{low}}_{pK^-}$ and $M^{\text{high}}_{pK^-}$ variables, which are the lower and higher values among M_{12} and M_{13} [89] due to their different energies. Therefore, when fitting the invariant mass spectrum of pK^-, the limits of the integral in Eq. (22) are described by Fig. 4, which are similar to what has been done in Ref. [75]. In fact, due to two identical kaons, the regions M^{low}_{12} and M^{high}_{12}, as

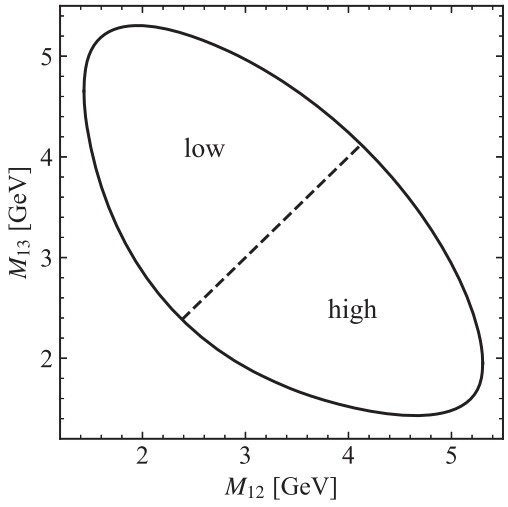

FIG. 4. Dalitz plot with the definitions of the regions M^{low}_{12} and M^{high}_{12}.

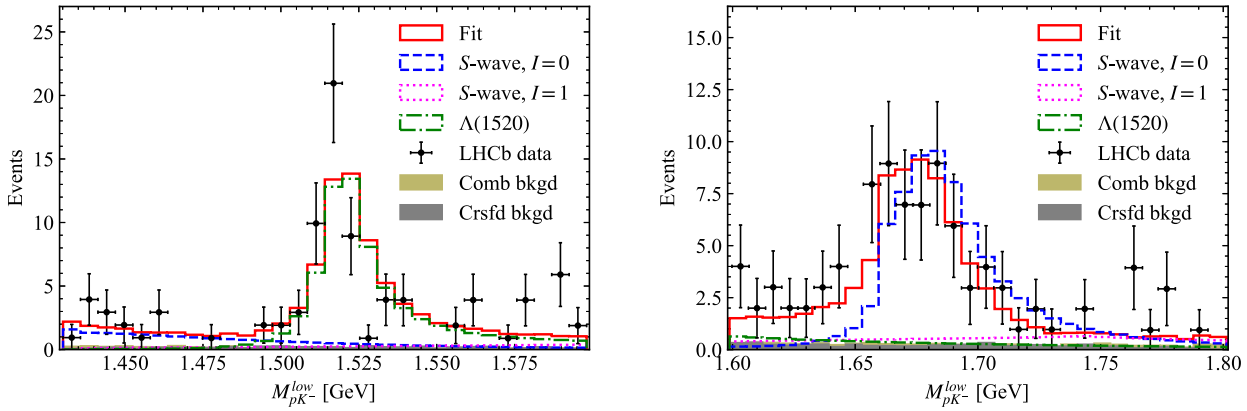

(a) The invariant mass distributions of lower pK^- in $[1.43, 1.60]$ GeV.

(b) The invariant mass distributions of lower pK^- in $[1.60, 1.80]$ GeV.

FIG. 5. The invariant mass distributions of lower pK^- in the $\Xi_b^- \to pK^-K^-$ decay. The solid (red) line is the total contributions of the S-wave with isospin $I = 0$ and $I = 1$, the $\Lambda(1520)$ and the background. The dashed (blue) and dotted (magenta) lines are the contributions from the S-wave with isospins $I = 0$ and $I = 1$, respectively. The dash-dot (green) line is the $\Lambda(1520)$ contributions. The dots (black) are the LHCb experimental data, the dark khaki and gray histograms are the combinatorial (Comb) and cross feed (Crsfd) backgrounds, respectively, which all are taken from Ref. [32].

shown in Fig. 4, could also be for the variable of M_{13}. Thus, when one folds the symmetry parts of Fig. 4 along $M_{12} = M_{13}$, all the data can be described by the folded Dalitz plot, which is really done in the experiments [32] with $m_{\rm low}$ and $m_{\rm high}$.

In our calculation, only two free parameters need to be determined by fitting the experimental data, i.e., $\mathcal{D}$ and $\mathcal{D}_{\Lambda(1520)}$, which represent the strength of the S-wave FSI and the $\Lambda(1520)$ in the D-wave, respectively. They are uncorrelated and do not affect the line shape of their invariant mass spectra. First, we make a combined fit of the LHCb experimental data as shown Fig. 5, and the fitted parameters and χ^2/dof are given in Table III. We can see that our results are in agreement with the experimental data. Note that we only use one set of (two) parameters, see Table III, and obtain good description for the two sets of experimental data of Figs. 5(a) and 5(b). In Fig. 5(a), above the pK^- threshold, the contributions from the resonance $\Lambda(1405)$ are generated by the coupled channel interactions of the S-wave with isospin $I = 0$ using the ChUA, which are shown by the dashed (blue) line. In the middle-energy region, as shown by the dash-dot (green) line, the structure of the $\Lambda(1520)$ state is clear. As shown in Fig. 5(b) for the lower pK^- invariant mass distributions from 1.6 GeV to 1.8 GeV, the contributions from the $\Lambda(1670)$ state is particularly visible, which is also dynamically generated in the S-wave FSI, recalling that there is no contribution from the tree-level diagram. As analyzed in Ref. [61], the $\Lambda(1405)$ corresponds to two states; the one with higher mass is a pure $\bar{K}N$ molecule, and the other one is a compositeness of the main components of $\pi\Sigma$ and small part of $\bar{K}N$, while the $\Lambda(1670)$ is a bound state of $K\Xi$. In Fig. 5(b), the peak structures in the total (solid, red) line and the one (dashed, blue) in the S-wave FSI with isospin $I = 0$ have obvious horizontal dislocation, while the $\Lambda(1520)$ has almost no contribution. This differences between them indicate that there will be another resonance contributed in the S-wave FSI with isospin $I = 1$, see the dotted (magenta) line and the following analysis.

Next, we plot the pK^- and K^-K^- invariant mass distributions in the full energy regions for the decay of $\Xi_b^- \to pK^-K^-$, see the results of Fig. 6. Thus, the horizontal axis of M_{pK^-} in Fig. 6(a) is in fact the full-energy range of M_{12}, $M_{12}^{\rm low} + M_{12}^{\rm high}$, whereas, the one in Fig. 6(c) is for the region of $M_{12}^{\rm low} < 2.05$ GeV. The results of Fig. 6(a) are consistent with the line shapes as shown in Figs. 7–11 of Ref. [32], where we do not compare these experimental results with events one parts by one parts due to the higher-energy region out of our concern as discussed in the introductions. In Fig. 6(a) the peak structures near the pK^- threshold are contributed by the amplitudes of the S-wave FSI and the D-wave $\Lambda(1520)$, and the structures in

TABLE III. Values of the parameters from the fit.

Parameters	$\mathcal{D}$	$\mathcal{D}_{\Lambda(1520)}$	χ^2/dof
Fit results	810.08 ± 22.79	1.70 ± 0.04	$86.38/(46-2) = 1.96$

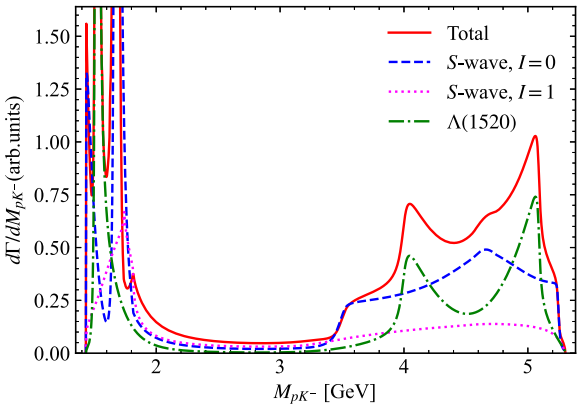

(a) The invariant mass distributions of pK^-.

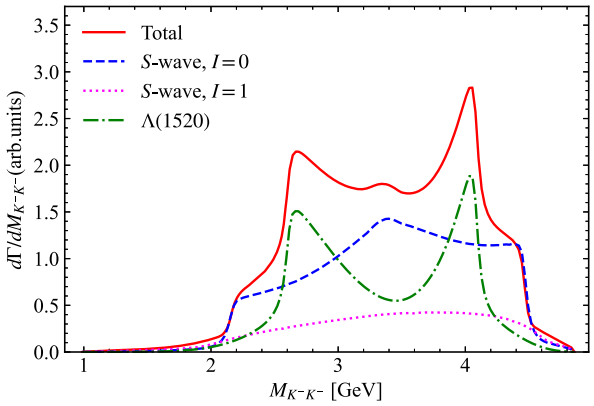

(b) The invariant mass distributions of K^-K^-.

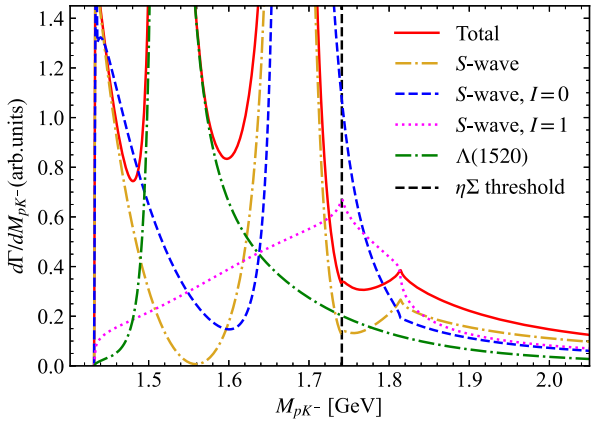

(c) The invariant mass distributions of pK^- in the low-energy region.

FIG. 6. The invariant mass distributions of pK^- and K^-K^- for the $\Xi_b^- \to pK^-K^-$ decay. The results for different lines are the same as Fig. 5. Furthermore, the dash-dot (goldenrod) line is the total contributions of the S-wave with isospins $I = 0$ and $I = 1$, the dashed (black) vertical line is the threshold of $\eta\Sigma$ channel.

the high-energy region are caused by the reflections of the resonance structures which appeared in the low-energy region. It is not surprising that there are two-peak structures for the contributions from the D-wave $\Lambda(1520)$, where a Breit-Wigner type amplitude is taken for its contribution of the D-wave, see Eq. (20), and which were also shown in the fitting results of Refs. [32,90,91]. Indeed, the Breit-Wigner type amplitude will also show up some peak structures when it is projected to the higher-energy region or the other energy variables, see more discussions in Ref. [92]. For the invariant mass spectrum of K^-K^- in Fig. 6(b), the main contributions also come from the reflections of the amplitudes of the $\Lambda(1520)$ and the FSI with isospins $I = 0$, 1, of which the line shape is similar to the part in the high-energy region of Fig. 6(a). Figure 6(c) shows more detailed structures in the low-energy region of Fig. 6(a). In Fig. 6(c), except for the obvious structures of the states $\Lambda(1405)$, $\Lambda(1520)$, and $\Lambda(1670)$, there is another resonance appearing in the FSI with isospin $I = 1$. The peak of this state is close to the threshold of $\eta\Sigma$ channel and has a typical cusp effect, which spans from the pK^- threshold to about 2 GeV, and leads to a small horizontal dislocation in the line shape of the total invariant mass spectrum and the one of S-wave FSI with isospin $I = 0$, see the solid (red) and dashed (blue) lines, respectively, as shown in Figs. 5(b) and 6(c). As done in Ref. [61], to extrapolate the scattering amplitudes to the general second Riemann sheet, we found a pole $\sqrt{s_p} = (1579.52 + 264.40i)$ MeV in the isospin $I = 1$ sector, which has total angular momentum $J = 1/2$ and is in agreement with the one $\sqrt{s_p} = (1579 + 264i)$ MeV found in Refs. [52,93,94]. Unfortunately, this resonance was not found in the experiments [32]. In fact, this new state with $I = 1$ is difficult to be detected in the present Ξ_b^- decay process, since its signal is destroyed totally by the interference effects from the states $\Lambda(1405)$

and $\Lambda(1670)$, as shown in the total results of Fig. 6(c). Since this state is below the $\eta\Sigma$ threshold, which couples strongly to the $K\Xi$ channel [52,93,94] and can decay into the $\bar{K}N$, $\pi\Sigma$, and $\pi\Lambda$ channels in the isospin $I=1$ sector. Therefore, some decay processes of the heavy hadrons, such as Λ_b and Ξ_b baryons, B and B_s mesons, which contain these final states of $\bar{K}N$, $\pi\Sigma$, and $\pi\Lambda$, may be detected for this new state. Thus, more accurate experimental results are needed to find it in the future.

Furthermore, we calculate the branching fractions of the corresponding decay channel. In our model, we do not know the weak-interaction vertex factor V_P in Eq. (7) and the couplings in Eq. (17). Therefore we use the experimentally measured branching fraction of the decay channel via $\Lambda(1520)$ as the known input to calculate the branching fractions of the decay channels via other resonances. In the evaluations, except for the vertex factor and the couplings, there is also a global constant C, which can be eliminated by calculating the ratio as below. By integrating the pK^- invariant mass distributions of the dashed (blue) line for the $\Lambda(1405)$ and the dash-dot (green) line for the $\Lambda(1520)$ in Fig. 6(c) we obtain the ratio,

$$\frac{\mathcal{B}(\Xi_b^- \to \Lambda(1405)K^-, \Lambda(1405) \to pK^-)}{\mathcal{B}(\Xi_b^- \to \Lambda(1520)K^-, \Lambda(1520) \to pK^-)} = 0.24^{+0.04}_{-0.02}, \quad (23)$$

where the integration limits for $\Xi_b^- \to \Lambda(1405)K^-$ decay are taken from the pK^- threshold up to 1.6 GeV, and the ones for $\Xi_b^- \to \Lambda(1520)K^-$ decay from the pK^- threshold up to 1.8 GeV. The uncertainties come from the changes of upper limits, 1.6 ± 0.05 GeV and 1.8 ± 0.05 GeV. Analogously, we get the following fractions

$$\frac{\mathcal{B}(\Xi_b^- \to \Lambda(1670)K^-, \Lambda(1670) \to pK^-)}{\mathcal{B}(\Xi_b^- \to \Lambda(1520)K^-, \Lambda(1520) \to pK^-)} = 1.12^{+0.03}_{-0.04}, \quad (24)$$

$$\frac{\mathcal{B}(\Xi_b^- \to RK^-, R \to pK^-)}{\mathcal{B}(\Xi_b^- \to \Lambda(1520)K^-, \Lambda(1520) \to pK^-)} = 0.40^{+0.01}_{-0.01}, \quad (25)$$

where R represents the state from FSI with isospin $I=1$ as discussed above. The integration limits for the $\Xi_b^- \to \Lambda(1670)K^-$ decay taken from 1.6 GeV up to 1.9 GeV, where the uncertainties come from the changes of lower limits 1.6 ± 0.05 GeV. The ones for the $\Xi_b^- \to RK^-$ decay from the pK^- threshold up to 2 GeV, where the uncertainties come from the changes of upper limits 2 ± 0.05 GeV. The decay branching fraction measured by the LHCb Collaboration experiment is $\mathcal{B}(\Xi_b^- \to \Lambda(1520)K^-, \Lambda(1520) \to pK^-) = (7.6 \pm 0.9 \pm 0.8 \pm 3.0) \times 10^{-7}$ [32], and then combining the above values in Eqs. (23)–(25), we obtain the other three branching fractions

$$\begin{aligned}
\mathcal{B}(\Xi_b^- \to \Lambda(1405)K^-, \Lambda(1405) \to pK^-) &= (1.80 \pm 0.76^{+0.30}_{-0.18}) \times 10^{-7}, \\
\mathcal{B}(\Xi_b^- \to \Lambda(1670)K^-, \Lambda(1670) \to pK^-) &= (8.51 \pm 3.62^{+0.20}_{-0.33}) \times 10^{-7}, \\
\mathcal{B}(\Xi_b^- \to RK^-, R \to pK^-) &= (3.08 \pm 1.31^{+0.08}_{-0.10}) \times 10^{-7}, \quad (26)
\end{aligned}$$

where the first uncertainties are estimated from the experimental errors of $\mathcal{B}(\Xi_b^- \to \Lambda(1520)K^-, \Lambda(1520) \to pK^-)$, and the second ones are estimated from the integrations in Eqs. (23)–(25). The following results are measured by the LHCb Collaboration [32],

$$\begin{aligned}
\mathcal{B}(\Xi_b^- \to \Lambda(1405)K^-, \Lambda(1405) \to pK^-) &= (1.9 \pm 0.6 \pm 0.7 \pm 0.7) \times 10^{-7}, \\
\mathcal{B}(\Xi_b^- \to \Lambda(1670)K^-, \Lambda(1670) \to pK^-) &= (4.5 \pm 0.7 \pm 1.3 \pm 1.8) \times 10^{-7}. \quad (27)
\end{aligned}$$

For the $(\Xi_b^- \to \Lambda(1405)K^-, \Lambda(1405) \to pK^-)$ decay, the theoretical value is consistent with the experiment within the uncertainties. We can see that even though the central values of our branching fraction of $(\Xi_b^- \to \Lambda(1670)K^-, \Lambda(1670) \to pK^-)$ decay is about two times larger than the one of the LHCb Collaboration measured, our result is consistent with the measurement within the uncertainties. For the predicted branching ratio corresponding to the resonance generated by the FSI with isospin $I=1$, further experimental measurements are hopefully performed.

IV. CONCLUSIONS

The three-body decay of $\Xi_b^- \to pK^-K^-$ is studied by taking into account the final state interactions based on the chiral unitary approach. The dominant Feynman diagram contributions from the W-external emission mechanism are considered in the weak-decay process. Our analysis shows that the final states pK^- can not be directly produced in the S-wave at the tree level, and the rescattering effect of the final states is mandatory. We also take into account the contributions from the state $\Lambda(1520)$ using the

corresponding effective Lagrangian. Our fitting results for the invariant mass distributions of lower pK^- are consistent with the experimental data. Then we present the detailed pK^- invariant mass spectra, where the resonances $\Lambda(1405)$ and $\Lambda(1670)$ are dynamically reproduced in the S-wave final state interactions with the isospin $I = 0$, which indicates the molecular nature of these two states. In addition, we find the contributions in the invariant mass distributions from a structure with isospin $I = 1$, of which the pole is located at $\sqrt{s_p} = (1579.52 + 264.40i)$ MeV. However, this state has not yet been observed experimentally. As discussed in Refs. [52,93,94], this resonance is strongly coupled to the $K\Xi$ channel, too. Furthermore, we calculate the branching ratios of the corresponding decay channels. The result of the branching fraction $\mathcal{B}(\Xi_b^- \to \Lambda(1405)K^-, \Lambda(1405) \to pK^-)$ is consistent with the measurements of the LHCb Collaboration within the uncertainties, while the one of $\mathcal{B}(\Xi_b^- \to \Lambda(1670)K^-, \Lambda(1670) \to pK^-)$ is a little bigger than theirs. We hope that the future experiments could search for the predicted resonance around 1580 MeV with isospon $I = 1$ and make further measurements for its corresponding branching fraction.

ACKNOWLEDGMENTS

We would like to thank En Wang and Pei-Rong Li for valuable discussions. This work is supported by the China National Funds for Distinguished Young Scientists under Grant No. 11825503, National Key Research and Development Program of China under Contract No. 2020YFA0406400, the 111 Project under Grant No. B20063, the National Natural Science Foundation of China under Grant No. 12047501, and by the Fundamental Research Funds for the Central Universities.

[1] R. Aaij *et al.* (LHCb Collaboration), Phys. Rev. Lett. **115**, 072001 (2015).
[2] R. Aaij *et al.* (LHCb Collaboration), Chin. Phys. C **40**, 011001 (2016).
[3] R. Aaij *et al.* (LHCb Collaboration), Phys. Rev. Lett. **117**, 082002 (2016).
[4] R. Aaij *et al.* (LHCb Collaboration), Phys. Rev. Lett. **117**, 082003 (2016).
[5] R. Aaij *et al.* (LHCb Collaboration), Phys. Rev. Lett. **122**, 222001 (2019).
[6] S. B. Yang *et al.* (Belle Collaboration), Phys. Rev. Lett. **117**, 011801 (2016).
[7] R. Aaij *et al.* (LHCb Collaboration), J. High Energy Phys. 05 (2016) 081.
[8] M. Ablikim *et al.* (BESIII Collaboration), Phys. Rev. Lett. **117**, 232002 (2016).
[9] R. Aaij *et al.* (LHCb Collaboration), J. High Energy Phys. 05 (2017) 030.
[10] R. Aaij *et al.* (LHCb Collaboration), J. High Energy Phys. 03 (2018) 043.
[11] M. Ablikim *et al.* (BESIII Collaboration), Phys. Rev. D **99**, 032010 (2019).
[12] J. Y. Lee *et al.* (Belle Collaboration), Phys. Rev. D **103**, 052005 (2021).
[13] H. X. Chen, W. Chen, X. Liu, and S. L. Zhu, Phys. Rep. **639**, 1 (2016).
[14] A. Hosaka, T. Iijima, K. Miyabayashi, Y. Sakai, and S. Yasui, Prog. Theor. Exp. Phys. **2016**, 062C01 (2016).
[15] A. Esposito, A. Pilloni, and A. D. Polosa, Phys. Rep. **668**, 1 (2016).
[16] F. K. Guo, C. Hanhart, U.-G. Meißner, Q. Wang, Q. Zhao, and B. S. Zou, Rev. Mod. Phys. **90**, 015004 (2018).
[17] S. L. Olsen, T. Skwarnicki, and D. Zieminska, Rev. Mod. Phys. **90**, 015003 (2018).
[18] N. Brambilla, S. Eidelman, C. Hanhart, A. Nefediev, C. P. Shen, C. E. Thomas, A. Vairo, and C. Z. Yuan, Phys. Rep. **873**, 1 (2020).
[19] M. Sumihama *et al.* (Belle Collaboration), Phys. Rev. Lett. **122**, 072501 (2019).
[20] R. Aaij *et al.* (LHCb Collaboration), Phys. Rev. Lett. **123**, 152001 (2019).
[21] R. Aaij *et al.* (LHCb Collaboration), J. High Energy Phys. 06 (2020) 136.
[22] R. Aaij *et al.* (LHCb Collaboration), Phys. Lett. B **772**, 265 (2017).
[23] H. X. Chen, L. S. Geng, W. H. Liang, E. Oset, E. Wang, and J. J. Xie, Phys. Rev. C **93**, 065203 (2016).
[24] J. J. Wu, R. Molina, E. Oset, and B. S. Zou, Phys. Rev. Lett. **105**, 232001 (2010).
[25] J. J. Wu, R. Molina, E. Oset, and B. S. Zou, Phys. Rev. C **84**, 015202 (2011).
[26] E. Santopinto and A. Giachino, Phys. Rev. D **96**, 014014 (2017).
[27] R. Chen, J. He, and X. Liu, Chin. Phys. C **41**, 103105 (2017).
[28] R. Aaij *et al.* (LHCb Collaboration), Sci. Bull. **66**, 1278 (2021).
[29] R. Aaij *et al.* (LHCb Collaboration), Phys. Rev. D **104**, L091102 (2021).
[30] R. Aaij *et al.* (LHCb Collaboration), Phys. Rev. Lett. **118**, 182001 (2017).
[31] J. Yelton *et al.* (Belle Collaboration), Phys. Rev. D **97**, 051102 (2018).
[32] R. Aaij *et al.* (LHCb Collaboration), Phys. Rev. D **104**, 052010 (2021).
[33] R. Aaij *et al.* (LHCb Collaboration), Phys. Rev. Lett. **118**, 071801 (2017).
[34] Z. H. Zhang and X. H. Guo, J. High Energy Phys. 07 (2021) 177.

[35] R. Sinha, S. Roy, and N. G. Deshpande, Phys. Rev. Lett. **128**, 081803 (2022).
[36] R. H. Dalitz and S. F. Tuan, Phys. Rev. Lett. **2**, 425 (1959).
[37] R. H. Dalitz and S. F. Tuan, Ann. Phys. (N.Y.) **10**, 307 (1960).
[38] M. H. Alston, L. W. Alvarez, P. Eberhard, M. L. Good, W. Graziano, H. K. Ticho, and S. G. Wojcicki, Phys. Rev. Lett. **6**, 698 (1961).
[39] N. Isgur and G. Karl, Phys. Rev. D **18**, 4187 (1978).
[40] S. Capstick and N. Isgur, Phys. Rev. D **34**, 2809 (1986).
[41] U. Loring, B. C. Metsch, and H. R. Petry, Eur. Phys. J. A **10**, 447 (2001).
[42] V. Crede and W. Roberts, Rep. Prog. Phys. **76**, 076301 (2013).
[43] T. Nakamura, J. Sugiyama, T. Nishikawa, M. Oka, and N. Ishii, Phys. Lett. B **662**, 132 (2008).
[44] N. Kaiser, P. B. Siegel, and W. Weise, Nucl. Phys. **A594**, 325 (1995).
[45] N. Kaiser, T. Waas, and W. Weise, Nucl. Phys. **A612**, 297 (1997).
[46] E. Oset and A. Ramos, Nucl. Phys. **A635**, 99 (1998).
[47] J. A. Oller and E. Oset, Nucl. Phys. **A620**, 438 (1997); **A652**, 407(E) (1999).
[48] J. A. Oller, E. Oset, and A. Ramos, Prog. Part. Nucl. Phys. **45**, 157 (2000).
[49] J. A. Oller and U.-G. Meißner, Phys. Lett. B **500**, 263 (2001).
[50] T. Hyodo, D. Jido, and A. Hosaka, Phys. Rev. C **78**, 025203 (2008).
[51] E. Oset, L. S. Geng, D. Gamermann, M. J. Vicente Vacas, D. Strottman, K. P. Khemchandani, A. Martinez Torres, J. A. Oller, L. Roca, and M. Napsuciale, Int. J. Mod. Phys. E **18**, 1389 (2009).
[52] E. Oset, A. Ramos, and C. Bennhold, Phys. Lett. B **527**, 99 (2002); **530**, 260(E) (2002).
[53] P. J. Fink, Jr., G. He, R. H. Landau, and J. W. Schnick, Phys. Rev. C **41**, 2720 (1990).
[54] D. Jido, A. Hosaka, J. C. Nacher, E. Oset, and A. Ramos, Phys. Rev. C **66**, 025203 (2002).
[55] D. Jido, J. A. Oller, E. Oset, A. Ramos, and U.-G. Meißner, Nucl. Phys. **A725**, 181 (2003).
[56] C. Garcia-Recio, M. F. M. Lutz, and J. Nieves, Phys. Lett. B **582**, 49 (2004).
[57] T. Hyodo and W. Weise, Phys. Rev. C **77**, 035204 (2008).
[58] Y. Ikeda, T. Hyodo, and W. Weise, Phys. Lett. B **706**, 63 (2011).
[59] Y. Ikeda, T. Hyodo, and W. Weise, Nucl. Phys. **A881**, 98 (2012).
[60] Z. H. Guo and J. A. Oller, Phys. Rev. C **87**, 035202 (2013).
[61] Z. Y. Wang, H. A. Ahmed, and C. W. Xiao, Eur. Phys. J. C **81**, 833 (2021).
[62] J. X. Lu, L. S. Geng, M. Doering, and M. Mai, arXiv:2209.02471.
[63] A. Starostin *et al.* (Crystal Ball Collaboration), Phys. Rev. C **64**, 055205 (2001).
[64] X. H. Zhong and Q. Zhao, Phys. Rev. C **79**, 045202 (2009).
[65] R. Manweiler, R. V. Cadman, H. Spinka, V. V. Abaev, D. Allen, C. E. Allgower, J. Alyea, M. A. Bates, V. S. Bekrenev, W. J. Briscoe *et al.*, Phys. Rev. C **77**, 015205 (2008).
[66] K. Miyahara and T. Hyodo, Phys. Rev. C **98**, 025202 (2018).
[67] K. Miyahara, T. Hyodo, and E. Oset, Phys. Rev. C **92**, 055204 (2015).
[68] L. Roca, M. Mai, E. Oset, and U.-G. Meißner, Eur. Phys. J. C **75**, 218 (2015).
[69] J. J. Xie and L. S. Geng, Eur. Phys. J. C **76**, 496 (2016).
[70] J. J. Xie, W. H. Liang, and E. Oset, Phys. Lett. B **777**, 447 (2018).
[71] E. Oset, W. H. Liang, M. Bayar, J. J. Xie, L. R. Dai, M. Albaladejo, M. Nielsen, T. Sekihara, F. Navarra, L. Roca *et al.*, Int. J. Mod. Phys. E **25**, 1630001 (2016).
[72] L. L. Chau, Phys. Rep. **95**, 1 (1983).
[73] L. L. Chau and H. Y. Cheng, Phys. Rev. D **36**, 137 (1987).
[74] K. Miyahara, T. Hyodo, M. Oka, J. Nieves, and E. Oset, Phys. Rev. C **95**, 035212 (2017).
[75] L. Roca and E. Oset, Phys. Rev. D **103**, 034020 (2021).
[76] R. P. Pavao, W. H. Liang, J. Nieves, and E. Oset, Eur. Phys. J. C **77**, 265 (2017).
[77] W. H. Liang and E. Oset, Phys. Lett. B **737**, 70 (2014).
[78] H. A. Ahmed, Z. Y. Wang, Z. F. Sun, and C. W. Xiao, Eur. Phys. J. C **81**, 695 (2021).
[79] A. Pich, Rep. Prog. Phys. **58**, 563 (1995).
[80] G. Ecker, Prog. Part. Nucl. Phys. **35**, 1 (1995).
[81] V. Bernard, N. Kaiser, and U.-G. Meißner, Int. J. Mod. Phys. E **04**, 193 (1995).
[82] J. K. Ahn, S. Yang, and S. I. Nam, Phys. Rev. D **100**, 034027 (2019).
[83] S. Y. Choi, T. Lee, and H. S. Song, Phys. Rev. D **40**, 2477 (1989).
[84] H. Haberzettl, C. Bennhold, T. Mart, and T. Feuster, Phys. Rev. C **58**, R40 (1998).
[85] R. M. Davidson and R. Workman, Phys. Rev. C **63**, 025210 (2001).
[86] H. Toki, C. Garcia-Recio, and J. Nieves, Phys. Rev. D **77**, 034001 (2008).
[87] P. A. Zyla *et al.* (Particle Data Group), Prog. Theor. Exp. Phys. **2020**, 083C01 (2020).
[88] E. Wang, H. X. Chen, L. S. Geng, D. M. Li, and E. Oset, Phys. Rev. D **93**, 094001 (2016).
[89] R. Aaij *et al.* (LHCb Collaboration), J. High Energy Phys. 04 (2019) 063.
[90] Z. Y. Wang, J. Y. Yi, Z. F. Sun, and C. W. Xiao, Phys. Rev. D **105**, 016025 (2022).
[91] Z. Y. Wang, H. A. Ahmed, and C. W. Xiao, Phys. Rev. D **105**, 016030 (2022).
[92] J. Z. Wang, D. Y. Chen, X. Liu, and T. Matsuki, Phys. Lett. B **817**, 136345 (2021).
[93] A. Ramos, E. Oset, and C. Bennhold, Nucl. Phys. **A721**, C711 (2003).
[94] F. Y. Dong, B. X. Sun, and J. L. Pang, Chin. Phys. C **41**, 074108 (2017).